Available online at www.sciencedirect.com
ScienceDirect
Journal of the European Ceramic Society 29 (2009) 317–322
www.elsevier.com/locate/jeurceramsoc

Role of powder properties and shaping techniques on the formation of pore-free YAG materials

Laura Esposito *, Andreana Piancastelli

ISTEC-CNR, Institute of Science and Technology for Ceramics, Faenza, Italy

Available online 2 June 2008

Abstract

A key feature of transparent ceramics is the absence of residual porosity because boundary between pores and ceramic grains is the origin for light scattering. Powders characterized by a grain size in the nanometric range are generally adopted for obtaining transparent ceramics because of their superior reactivity, but the formation of undesired secondary phase related to the presence of impurities, is observed. The present study shows the results obtained with alternative, highly pure, micrometric powders with two shaping techniques, cold isostatic pressing (CIP) and slip casting (SC). The powder treatment and shaping process are easier when coarser powders are adopted. The influence of the powder properties and of the dispersant system on the particle packing, on the density and on the porosity are studied in relation to the two shaping techniques. The role of the aforementioned features on the final microstructure and on the optical properties are also discussed.

Keywords: YAG; Shaping; Zeta potential; Sintering; Optical properties

1. Introduction

Transparent YAG ($Y_3Al_5O_{12}$) based ceramics are generally obtained with nanometric powders prepared following complex chemical routes.[1–6] Nanometric powders exhibit a high reactivity during the sintering process but on the other hand are difficult to manipulate. This feature may lead to the contamination with undesired impurities or to the mixture of powders in a different ratio with respect to the desired stoichiometry. In addition, the formation of other crystalline phases beside YAG may occur. As an example in Fig. 1 the transparency and microstructure of a sample prepared with nanometric powders are revealed.[7] The formation of $Y_4(Al,Si,Nd)_2O_9$ grains is observed in this sample. Another problem encountered with nanometric powders is related to the difficulty to prepare slurries with the viscosity and stability needed for the slip casting (SC) technique, especially when different oxides are mixed together as in the case of the reactive sintering process.[8–10] On the other hand, slip casting is an attractive technique for laser source materials because complicated shapes can be obtained.[11,12] The present study shows the relationship of the shaping technique with the final density and residual porosity when micrometric powders characterized by a high level of purity are selected. If a proper particle packing and density are obtained during the shaping process, the closure of residual pores may be accomplished through the control of the grain growth during sintering, thus obtaining fully dense materials from micrometric powders. The results obtained with two shaping techniques, cold isostatic pressing (CIP) and SC, are discussed. The results in terms of microstructure and optical properties are also compared to those obtained with nanometric powders.

2. Experimental

The characteristics and morphology of the selected powders are revealed in Table 1 and Fig. 2, respectively. The powders for all the shaping techniques were mixed according to the stoichiometry $Nd_{0.024}Y_{2.976}Al_5O_{12}$ (0.8 at.% Nd:YAG). As sintering additive 0.5 wt% of tetraethyl-orthosilicate (TEOS) is used in all sintered samples. For the electroacoustic characterization water suspensions with a solid content of 5 vol.% were prepared by ball milling for 24 h. An automatic titrator software is used in order to evaluate the best amount of dispersant at spontaneously resulting pH (9.9 for Al_2O_3, 9.2 for Y_2O_3), i.e. the maximum value of zeta potential reached with the tested anionic dispersants, Duramax D3021 (Rhom and Haas), Dolapix PC 21 and PC 75 (Zschimmer and Schwarz). The amount of

* Corresponding author.
E-mail address: laura@istec.cnr.it (L. Esposito).

0955-2219/$ – see front matter © 2008 Elsevier Ltd. All rights reserved.
doi:10.1016/j.jeurceramsoc.2008.03.047

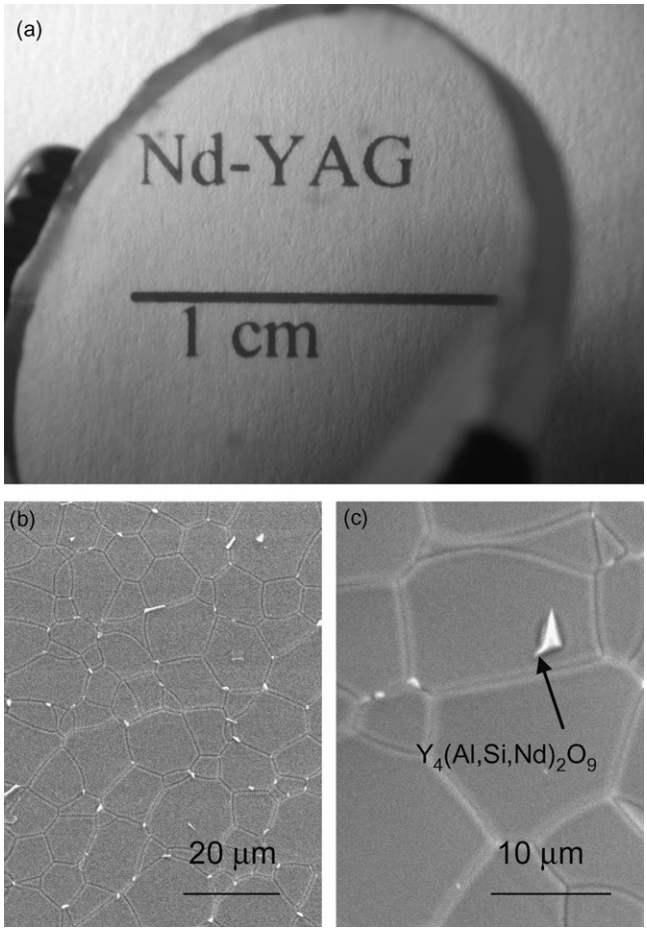

Fig. 1. Transparency (a) and SEM microstructure (b) of a Nd–YAG sample prepared with nanometric powders by cold isostatic pressing.[7] The sample is prepared following the same experimental procedure described for samples obtained with micrometric powders. Picture (a) shows the transparency given by the sample not in direct contact of a printed surface.

dispersant reported in table or graphs is expressed in wt% with respect to the ceramic powder. The reometer C-VOR Bohlin Instruments, was used for the reological characterization of the slurries. Gypsum moulds were used for SC. The slurries had a solid content of 80 wt% and were previously ball milled for 1–24 h. The powders for the CIP were wet ball milled in ethanol with 99.9% pure Al_2O_3 grinding media and dried with rotavapor. The obtained powders were linear pressed and finally CIP at 2500 bar. Pellets with a diameter of 1 cm and 2–4 mm thick are prepared. The porosity of the SC samples was measured after a debonding cycle at 1100 °C × 1 h (heating rate 100 °C/h) using a mercury intrusion porosimeter, Pascal 240, Thermo Finnigan. A slow debinding + air sintering cycle is adopted for the densification of the samples. In particular, in the temperature range between 300 and 600 °C a slow heating rate is used (50 °C/h). The sintering temperature is 1650 °C with a soaking time of 6 h. Vacuum sintering at 1750 °C × 4 h was also performed on selected CIP samples previously debinded at 1100 °C. The density of the as-cast samples is geometrically measured whereas the density of samples after sintering is measured in distilled water following the Archimedes method. The phases formed during the heating treatment are identified by X-ray powder

Table 1
Properties of the powders

Powder	Purity (%)	SSA (m^2/g)	D_{50} (µm)
Al_2O_3	99.99	17.22	0.20
Y_2O_3	99.999	7.56	3.91
Nd_2O_3	99.95	8.34	0.03–0.05[a]

Al_2O_3: Taimei TM-DAR. Y_2O_3: Alfa Aesar Reacton®. Nd_2O_3: China rare materials nano-Nd_2O_3. Purity levels are manufacturer's data. D_{50} of Nd_2O_3 powder refers to the crystallite size. Particle size distribution measured by SediGraph. Specific surface area (SSA) measured by BET method.

[a] Manufacturer data.

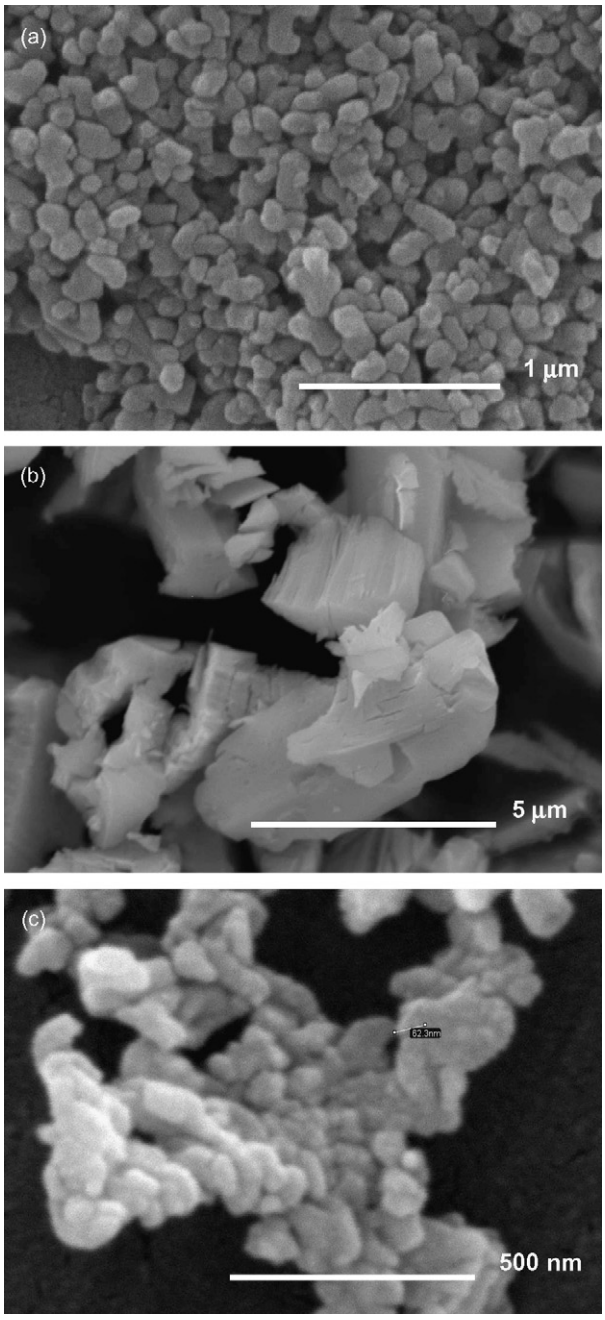

Fig. 2. Al_2O_3 Taimei TM-DAR (a), Y_2O_3 Alfa Aesar (b), Nd_2O_3 China rare materials (c).

diffraction (XRPD) (10–90° 2ϑ range, scan rate 0.02° 2ϑ, 5 s per step). Scanning electron microscopy (SEM) (Leica Cambridge Stereoscan 360) coupled with an energy-dispersive X-ray spectrometer (EDS) is used for the microstructure characterization. The laser transmission was measured at 1064 nm (i.e., one of the more typical laser emission wavelength of Nd:YAG when used as solid state laser source) and was performed at a distance of 1–4 mm (Vilnius University) on 1 μm mirror-polished samples.

3. Results

The SEM analysis of the powders revealed in Fig. 2 shows that Al_2O_3 and Nd_2O_3 have a quasi-spherical morphology whereas Y_2O_3 has an irregular morphology and is particularly coarse, as also confirmed by the SSA and D_{50} values revealed in Table 1. The Nd_2O_3 powder exhibits a low specific surface area value despite it is nanometric because it is highly aggregated. All powders exhibit a high purity level. In Fig. 3, the results obtained with the electroacoustic characterization are revealed. The zeta potential curves obtained with DOLAPIX PC75 are very similar to those obtained with PC21. In all the measures the positive starting zeta potential value becomes negative after the addition of a small amount of dispersant and reaches a plateaux value of about −60 mV. The amount of dispersant needed to reach the stabilization of the suspension is quite similar (0.3–0.5 wt%).

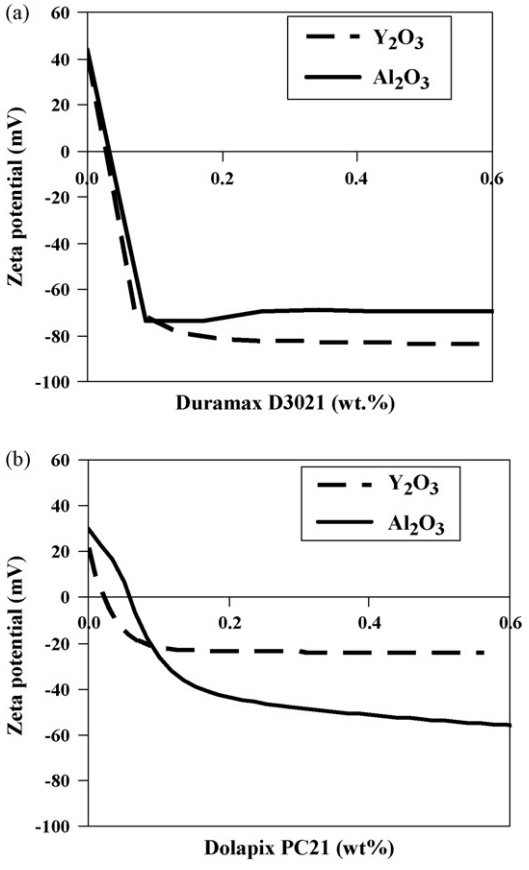

Fig. 3. Zeta potential curves of Al_2O_3 and Y_2O_3 suspensions with Duramax (a) and Dolapix (b) as dispersant.

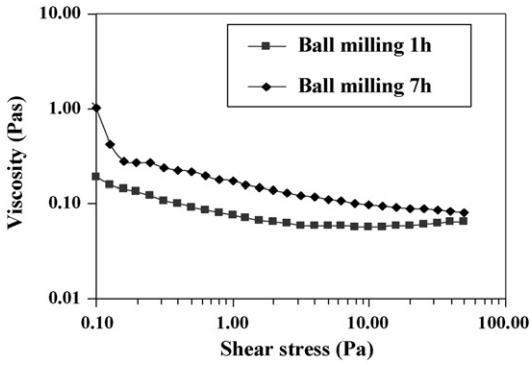

Fig. 4. Slurries prepared with Dolapix PC21 as dispersant.

The starting positive values of zeta potential is coherent with the surfaces of basic oxides that subtracts protons to the water where they are dispersed. The affinity of these surfaces for both dispersants is revealed by the immediate inverting of zeta potential already after the first additions. Further dispersant additions slightly increase the absolute value of zeta potential until a plateaux is reached, i.e., when the particle surface is fully coated. The related dispersant amount is considered the optimum one to stabilize the suspension. Any further addition would not be adsorbed and would negatively affect the stability of the suspension with depletion and/or flocculation phenomena.

On the basis of the electroacoustic results, Dolapix PC21 was selected for the reological measures and two slurries with 0.40 wt% of Dolapix PC21 and a solid content of 50 vol.% were ball milled for 1, 7 and 24 h, respectively. The resulting slurries exhibited the viscosity curves revealed in Fig. 4. The viscosity of the slurry ball milled for 24 h could not be measured because it was higher than the detection limit of the instrument. The porosity distribution of the samples obtained after slip casting of these slurries is revealed in Table 2. A higher viscosity, a higher overall porosity and a larger mean pore diameter is observed with the ball milling treatment of 7 versus 1 h. Moreover, the distribution of the pores in the slip cast samples is different. A higher amount of pores is found in the range between 2.0 and 0.1 μm in the sample obtained with the slurry ball milled for 7 h.

Table 3 reveals the characteristics of the samples selected for the sintering cycles. Two SC samples obtained from slurries prepared with 0.4 wt% of Dolapix PC21 (sample 1) and with 0.4% of Duramax D3021 (sample 2), are selected for the densification cycle in air. The obtained densities and microstructures are compared with those of CIP samples sintered in air and under vacuum.

Table 2
Porosities of slip cast samples obtained after ball milling of 1 and 7 h

Ball milling time (h)	Total porosity (%)	Pore Size distribution (%)		
		2.0–0.1[a]	0.1–0.05[a]	0.05–0.01[a]
1	32.54	0.82	82.24	16.94
7	34.40	5.56	88.05	6.39

The porosity is measured after a calcination cycle at 1100 °C × 1 h.
[a] Range (μm).

Table 3
Description of samples prepared for sintering

Sample	Dispersant	Forming technique	Sintering cycle and atmosphere
1	PC21	SC	1650 °C × 6 h, air
2	D3021	SC	1650 °C × 6 h, air
3	PEG 400	CIP	1650 °C × 6 h, air
4	PEG 400	CIP	1750 °C × 4 h, vac.

SC: slip casting. CIP: cold isostatic pressing. Samples 1 and 2 were ball milled for 1 and 24 h, respectively.

Table 4
Density and mean grain size of samples before and after sintering in air at 1650 °C × 6 h

Sample	Density (%)		Grain size (μm)	Pore size (μm)
	As-dried	As-sintered		
1	61.8	96.0	3–5	~6
2	62.8	98.9	10–12	~9
3	60.0	99.5	8–10	~4
4	60.0	100	10–15	~2
Ref.	–	100	1–2	–

The theoretical density of Nd:YAG is 4.55 g/cm^3. Grain and pore size are measured by the SEM image analysis. Ref.: material used as reference, 1.1 at.% Nd:YAG (Konoshima Chemical Co. Ltd.).

The results obtained after sintering in air are reported in Table 4 and in Fig. 5.

The density of SC samples before sintering is higher than the density of CIP samples, whereas after sintering the latter exhibit a higher density. Sample 1, despite the optimal viscosity of the slurry, exhibits a lower as-dried and sintered density, smaller grains and pores than sample 2. The latter sinters better but the not homogeneous particle packing obtained during casting leads to relatively large pores which survive after sintering. CIP samples have smaller pores than SC samples, whereas the grain size is similar despite the higher density.

Samples sintered in air are opaque whereas under vacuum and at a higher temperature different values of transparency are obtained. During sintering closed pores forms. The air pressure that builds up within the closed pores during sintering in air inhibits their closure. On the contrary if sintering is conducted under vacuum no pressure forms into the pores, which therefore close more easily. For this reason vacuum sintering generally enhances the pore closure.

Table 5
Laser transmission of samples @ 1064 nm wavelength

Sample	Transmission (%)				Average (%)
	1 mm	2 mm	3 mm	4 mm	
4	38.9	36.3	36.3	38.1	37.4
Sample of Fig. 1	78.3	78.1	78.1	76.1	77.6
Commercial Nd:YAG	84.5	84.3	84.3	84.3	84.4

Measures from Vilnius University (Prof. Valdas Sirutkaitis). The commercial Nd:YAG material used as reference is produced by Konoshima Chemical Co. Ltd. and contains 1.1 at.% of neodymium.

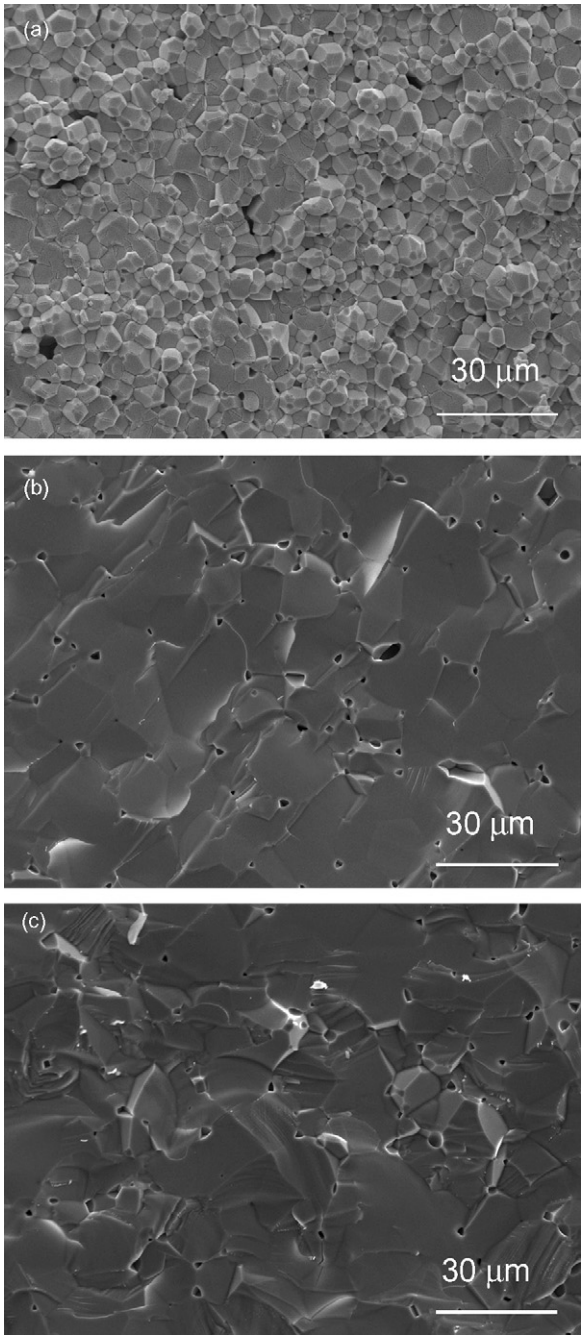

Fig. 5. Microstructure of the fracture surface of samples 1 (a), 2 (b) and 3 (c) after sintering in air (Table 4).

In Table 5, the laser transmission of sample 4 (Fig. 6) and of the sample prepared with nanometric powders (Fig. 1) are compared with the transmission of a commercial material.

Sample 4 exhibits a lower transmission than the sample obtained with nanometric powders. The latter sample, prepared by cold isostatic pressing under the same experimental condition of sample 4, contains less and smaller residual pores and these relate to the grain size.[9,13–15] On the other hand, sample 4 is a pure Nd:YAG material, whereas in case of the sample shown in Fig. 1 and prepared with nanometric powders, secondary phases formed during sintering.

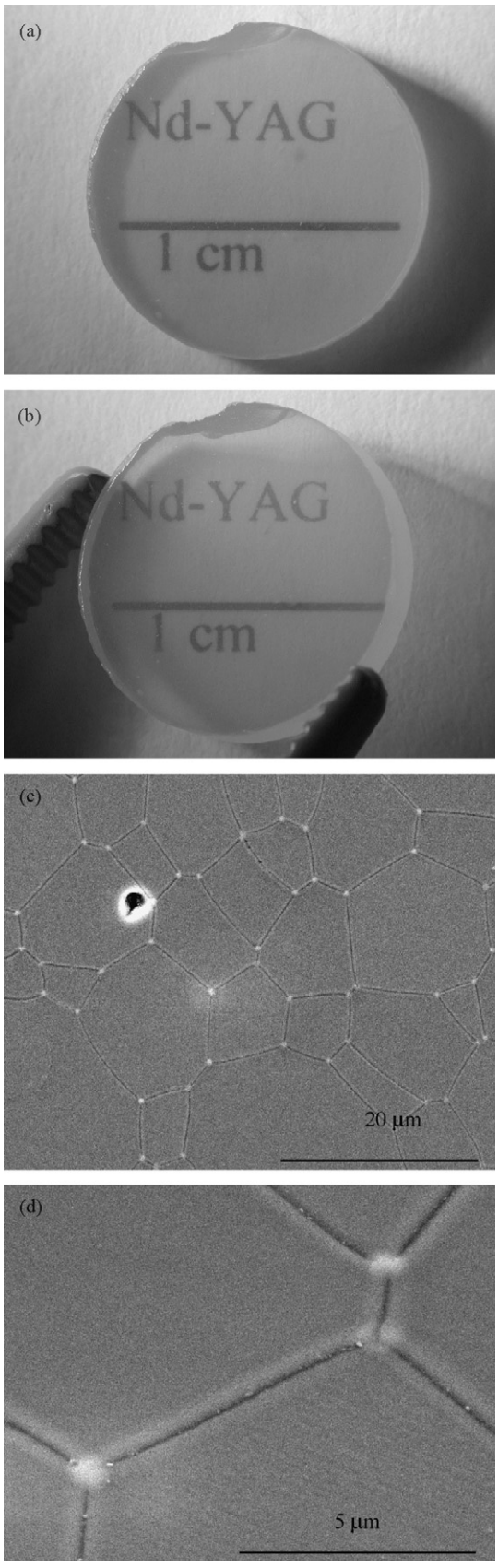

4. Discussion

The results obtained with the electroacoustic characterization show that the selected dispersants are suitable for the electrosteric stabilization of the slurries (Fig. 3). The viscosity measurement, however, showed that the ball milling process, in particular the ball milling duration, affects the slurry stabilization, probably by breaking the residual aggregates of the starting powders (Fig. 4), thus increasing the specific surface area. The consequent change of the slurry stabilization promotes an increase of the viscosity. A higher viscosity of the slurry inhibits an intimate particle packing during casting, as shown by the higher porosity and larger average pore size of the sample obtained with the slurry ball milled for longer time (Table 2).

The effect of the ball milling time on the particle packing can be evaluated even by comparing the characteristics of sample 1 and 2, Table 4. Sample 1, obtained from a well stabilized slurry, exhibit a lower density but smaller grain size and residual pores after sintering compared to sample 2, obtained from a slurry which was ball milled for 24 h (Fig. 5). A long ball milling improves the intimate mixing among the powders and therefore it is expected to enhance the sintering rate. In deed, sample 2 exhibits a higher density than sample 1, but the large pores from the casting process survive after sintering. On the other hand, sample 1 is fully transformed with no residual Al_2O_3 or Y_2O_3 grain, i.e. an intimate powder mixing was obtained even with the short ball milling treatment. These results show that the density value is not the sole parameter that must be considered in order to evaluate the quality of transparent materials. Transparency, a fundamental requirement for laser source materials, is affected by the residual pore size, not only by the overall amount of residual porosity. In particular, pores with dimensions smaller that the wavelength of the radiation allow its in-line transmission with no scattering effects.[3,14] The best results in terms of microstructure and transparency are obtained by cold isostatic pressing (Tables 4 and 5, Figs. 5 and 6). Sample 3 exhibits comparable grain size, a higher density and smaller residual pores as samples 1 and 2 sintered under the same heating conditions. If sintered under vacuum (sample 4), it exhibits a relatively high transmission value (Table 5). The best sample in terms of transparency is however the CIP-ed sample prepared with nanometric powders, which exhibits a pore-free microstructure (Fig. 1). On the basis of these results, it is necessary to improve the quality of the particle packing during shaping. This can be obtained through a better stabilization of the slurry for slip casting and

Fig. 6. Transparency (a and b) and SEM (c and d) pictures of sample 4 (Table 4). Picture (b) shows the tilted sample not in direct contact with a printed surface. The EDS analysis of the grain boundaries and of the triple points of this sample, even of the bright spots, does not evidence phases with a composition different than the expected Nd–YAG phase. The bright spots, not evidenced in the as-polished surface, should be a consequence of the migration of the heavier elements (Y and Nd) from the inner part of the material during the thermal etching treatment performed at 1350 °C. If so, the difference of composition is below the detection limit of the available EDS instrument.

by selecting other starting powders, in particular Y_2O_3 powder characterized by a more spherical morphology and a smaller grain size with respect to the powder used in the present study. In addition, shaping by CIP can be further improved with a dispersant which promotes the formation of a close particle packing.

5. Conclusions

The materials described in the present study and produced with micrometric powders by reactive sintering are fully YAG based materials. No additional phases or presence of impurities which may come from the powder contamination during the shaping treatment are found. Cold isostatic pressing promotes a better particle packing and consequently a higher density, lower porosity and smaller residual pores than slip casting. The latter is influenced by the ball milling duration. A long milling fastens the sintering process but increases the slurry viscosity with detrimental effects on the particle packing during casting and consequently on the final grain and pore size. The YAG based material obtained with nanometric powder exhibits a higher transparency related to the smaller grain and residual pores. On the other hand in this material the formation of undesired phases during sintering was observed. Improvements in the particle packing during cold isostatic pressing by selecting powders still in the micrometric range but not aggregated, finer and with a more spherical morphology than those used in the present study, may improve the transparency of materials by reducing the residual pore size.

Acknowledgements

This work was conducted in the frame of the European CRAFT Project NOVIGLAS Contract no. COOP-CT-2004-512318. The authors wish to thank Dr. Eckhard Sonntag, Broell GmbH & Co., for the useful suggestions and fruitful discussions and Prof. Valdas Sirutkaitis, Vilnius University, for the laser transmission measurements.

References

1. Ikesue, A. and Aung, Y. L., Synthesis and performance of advanced ceramic lasers. *J. Am. Ceram. Soc.*, 2006, **89**(6), 1936–1944.
2. Krell, A. and Hutzler, T., Transparent poly-crystalline sintered ceramic of cubic crystal structure. US Patent US 2005/0164867 A1, July 28, 2005.
3. Krell, A., Hutzler, T. and Klimke, J., Transparent ceramics for structural applications. Part 1. Physics of light transmission and technological consequences. *Ceram. Forum Int./Ber. DKG*, 2007, **84**(4), 345–351.
4. Rabinavitch, Y., Tétard, D., Faucher, M. D. and Pham-Thi, M., Transparent polycrystalline neodymium doped YAG: synthesis parameters, laser efficiency. *Opt. Mater.*, 2003, **24**.
5. Tachiwaki, T., Yoshinaka, M., Hirota, K., Ikegami, T. and Yamaguchi, O., Novel synthesis of $Y_3Al_5O_{12}$ (YAG) leading to transparent ceramics. *Solid State Commun.*, 2001, **119**, 603–606.
6. Hreniak, D. and Strek, W., Synthesis and optical properties of Nd^{3+}-doped $Y_3Al_5O_{12}$ nanoceramics. *J. Alloys Compd.*, 2002, **341**, 183–186.
7. Esposito, L. and Piancastelli, A., Nd–YAG polycrystalline ceramics by reactive sintering of nanometric powders, in preparation.
8. Costa, A. L., Esposito, L., Medri, V. and Bellosi, A., Synthesis of YAG-based Material using micrometric powders. *Adv. Eng. Mater.*, 2007, **9**(4), 307–312.
9. Esposito, L., Costa, A. L. and Medri, V., Reactive sintering of YAG-Based materials using micrometer-sized powders. *J. Eur. Ceram. Soc.*, 2008, **28**, 1065–1071.
10. Lee, S.-H., Kochawattana, S. and Messing, G., Solid-state reactive sintering of transparent polycrystalline Nd:YAG ceramics. *J. Am. Ceram. Soc.*, 2006, **89**(6), 1945–1950.
11. Takagimi, Y. and Hideki, Y., Rare earth garnet sintered compact. US Patent 2005/0215419 A1, September 29, 2005.
12. Lee, H. D., Mah, T., Parthasarathy, T. A. and Keller, K. A., YAG lasing systems and methods, US Patent 2005/0281302 A1, December 22, 2005.
13. Slamovich, E. B. and Lange, F., Densification of large pores. I. Experiments. *J. Am. Ceram. Soc.*, 1992, **75**(9), 2498–2508.
14. Ikesue, A. and Yoshida, K., Influence of pore volume on laser performance of Nd:YAG ceramics. *J. Mater. Sci.*, 1999, **34**, 1189–1195.
15. Ikesue, A., Yoshida, K., Yamamoto, T. and Yamaga, I., Optical scattering centers in polycrystalline Nd:YAG laser. *J. Am. Ceram. Soc.*, 1997, **80**(6), 1517–1522.